Mathematical Sciences Faculty Publications

2013

Tensor virial equation of evolving surfaces in sintering of aggregates of particles by diffusion

K. A. Brakke
Susquehanna University

F. Wakai
Tokyo Institute of Technology

Tensor virial equation of evolving surfaces in sintering of aggregates of particles by diffusion

F. Wakai [a,*], K.A. Brakke [b]

[a] Secure Materials Center, Materials and Structures Laboratory, Tokyo Institute of Technology, R3-23 4259 Nagatsuta, Midori, Yokohama 226-8503, Japan
[b] Mathematics Department, Susquehanna University, Selinsgrove, PA 17870-1164, USA

Abstract

The moment of inertia tensor is a quantity that characterizes the morphology of aggregates of particles. The deviatoric components indicate the anisotropy of the aggregate, and its compactness is described by the isotropic component, i.e. the second moment of inertia, which is related to the radius of gyration. The equation of motion of the moment of inertia tensor is proposed for the sintering and coalescence of crystalline particles by bulk diffusion and surface diffusion. Simulations of the evolution of aggregates of particles (linear chains, rings and branched chains) show that the aggregates become more compact and more isotropic structures, driven by the surface energy tensor or the surface force density. The tensor virial equation for diffusion is applicable also to evolution of pores, precipitates and inclusions embedded in a surrounding matrix.

© 2013 Acta Materialia Inc. Published by Elsevier Ltd. All rights reserved.

Keywords: Sintering; Simulation; Micromechanical modeling

1. Introduction

The tensor virial equation is the equation of motion of the moment of inertia tensor of an aggregate of particles [1]. It is obtained by first multiplying the force by position and then integrating the result over the volume of the system. While the usual scalar virial theorem applies to isotropic systems, the diagonal terms have application to anisotropic systems. The tensor virial equation is of interest in a wide variety of problems involving anisotropic isolated systems [2], for example, an aggregate of particles evolving under the action of surface tension. Chandrasekhar [3] and later Rosenkilde [4] introduced the surface energy tensor that plays an important role in the dynamics of the moment of inertia tensor.

The tensor virial method was applied to the spheroidization of a single particle in viscous sintering where inertia forces are negligible [5]. A non-spherical amorphous/glass particle relaxes to its equilibrium shape by viscous flow driven by capillarity. In this system the tensor virial equation gives a relation between the volume integral of the velocity gradient tensor (strain rate) and the surface energy tensor. The equation shows that the deformation of an isolated ellipsoidal particle is driven by the deviatoric component of the surface energy tensor in viscous sintering.

In the chemical synthesis of powders, coagulation and sintering result in the aggregation of primary particles. The morphology evolves from fractal-like open structures to compact structures by viscous sintering of amorphous multi-particle aggregates [6–8]. Both the surface area and the second moment of inertia of aggregates reduce in the morphological evolution [9,10].

The sintering of an aggregate of crystalline particles takes place by diffusion at elevated temperatures. It is well known that the shrinkage is a result of the relative motion of particles caused by grain boundary diffusion [11,12]. The thermodynamic driving force for shrinkage is the sintering force [13,14], and the sintering stress [15] that is expressed as a function of the surface energy tensor [16]. At the same

* Corresponding author. Tel.: +81 45 924 5361; fax: +81 45 924 5390.
E-mail address: wakai.f.aa@m.titech.ac.jp (F. Wakai).

time, each particle changes its shape by bulk diffusion [17,18], surface diffusion [19–21] and evaporation–condensation [22].

Neck formation between primary particles converts the agglomerates to aggregates. Sintering and coalescence make aggregates become more compact structures, even in the absence of grain boundary diffusion [14,23]. When the surface energy is isotropic, the bulk diffusion and surface diffusion make aggregates of crystalline particles become more isotropic structures. While the densification of bulk material is measured by the bulk density, the compactness of a multi-particle aggregate is defined by the second moment of inertia (radius of gyration) [10,24,25]. The anisotropy of the aggregate is evaluated by the deviatoric components of the moment of inertia tensor.

The objective of this paper is to show the equation of motion of the moment of inertia tensor for microstructural evolution. The structure of the paper is as follows. In Section 2, we consider tensor virial equations for bulk diffusion and surface diffusion. The anisotropic deformation by bulk diffusion is expressed as a response to the deviatoric components of the surface energy tensor. For sintering by surface diffusion, the thermodynamic driving force is identified in the equation of motion of the moment of inertia. Brakke's Surface Evolver program [26] is used as a tool to simulate the evolution of aggregates of particles (linear chains, rings and branched chains) by surface diffusion in Section 3. Although we treat only isolated aggregates in the present paper, the tensor virial equation for diffusion is applicable also to the morphological evolution of pores, cavities, precipitates and inclusions embedded in a surrounding matrix. The moment of inertia tensor will be a useful quantity to characterize the microstructural evolution (size, shape, anisotropy and orientation), because it is experimentally observable through the developments of three-dimensional imaging techniques: atom probe tomography [27], electron microscopy tomography [28], focused ion beam tomography [29] and X-ray tomography [30].

2. Dynamics of evolving interface

2.1. Bulk diffusion

Microstructural development involves evolving interfaces and surfaces. When matter is transferred to/from the bulk, the normal velocity v_n of the surface is proportional to the flux j_n normal to the surface:

$$v_n = j_n \Omega \tag{1}$$

where Ω is the atomic volume. The diffusive flux in the bulk is proportional to the gradient of a chemical potential μ:

$$\mathbf{j} = -\frac{D_L}{kT\Omega} \nabla \mu \tag{2}$$

where D_L is the diffusion coefficient in the bulk, k is the Boltzmann constant and T is the absolute temperature. Mass conservation in the bulk gives

$$\nabla^2 \mu = 0 \tag{3}$$

Herring [17,31] has shown that the chemical potential just below the surface is

$$\mu - \mu_0 = -\gamma_s \kappa \Omega \tag{4}$$

where μ_0 is the chemical potential under a flat surface and γ_s is the surface energy. The curvature κ, the sum of the principal curvatures (note this is twice the traditional definition of mean curvature), is expressed as the divergence of the unit (outward) normal vector n_i to the surface:

$$\kappa = -\partial n_k / \partial x_k \tag{5}$$

The summation convention for repeated indices is applied throughout this paper. The curvature is defined positive when the center of curvature is outside of the particle: it is negative $-2/r_0$ for a spherical particle with radius r_0.

We consider a body of uniform density with volume V enclosed by a surface A. The body may be a single isolated particle or an aggregate of particles. The moment of inertia tensor of the body about the position of the center of mass is defined by

$$I_{ij} = \int_V x_i x_j dV \tag{6}$$

Thus,

$$\frac{d}{dt} I_{ij} = \int_V (x_i v_j + v_i x_j) dV \tag{7}$$

where velocity is $v_i = dx_i/dt$. We regard the velocity field inside the particle as

$$v_i = j_i \Omega \tag{8}$$

From Eqs. (8) and (2), we obtain

$$\int_V x_j v_i dV = -\frac{D_L}{kT} \int_V x_j \frac{\partial \mu}{\partial x_i} dV \tag{9}$$

After integrating by parts, and using the divergence theorem, we have

$$\int_V x_j \frac{\partial \mu}{\partial x_i} dV = \int_A x_j \mu n_i dA - \delta_{ij} \int_V \mu dV \tag{10}$$

By substituting the boundary condition, Eq. (4), into Eq. (10), we obtain

$$\int_V x_j \frac{\partial \mu}{\partial x_i} dV = -\Omega \int_A \gamma_s \kappa n_i dA + \mu_0 \int_A x_j n_i dA - \delta_{ij}$$
$$\times \int_V \mu dV \tag{11}$$

From the identity

$$\int_A x_j n_i dA = \int_V \frac{\partial x_j}{\partial x_i} dV = V \delta_{ij} \tag{12}$$

the tensor virial equation for bulk diffusion takes the form

$$\frac{1}{V} \frac{d}{dt} I_{ij} = -\frac{2D_L \Omega}{kT} \left(\frac{2S_{ij}}{V} - \delta_{ij} \bar{p} \right) \tag{13}$$

where S_{ij} is the surface energy tensor that is expressed as [3,4]

$$S_{ij} \equiv -\frac{1}{2} \int_A \gamma_s x_j \kappa n_i dA = \frac{1}{2} \int_A \gamma_s (\delta_{ij} - n_i n_j) dA \quad (14)$$

From the identity $\delta_{ii} - n_i n_i = 2$, the trace of the surface energy tensor S_{ii} gives the total surface energy $\gamma_s A$. $\bar{p}$ is the equivalent pressure that corresponds to the mean chemical potential:

$$\bar{p} = \frac{1}{V} \int_V \frac{\mu - \mu_0}{\Omega} dV \quad (15)$$

The chemical potential inside the body is obtained by solving a Dirichlet problem (Eqs. (3) and (4)).

The moment of inertia tensor is separated into two parts: the isotropic component $I = I_{ii}/3$ and the deviatoric components $I'_{ij} \equiv I_{ij} - \delta_{ij} I$. The second moment of inertia $3I$ is related to the radius of gyration R_g, $R_g^2 = 3I/V$. The rate of decrease in the second moment of inertia is proportional to the difference between the Laplace pressure $2\gamma_s A/3V$ and the equivalent pressure

$$\frac{1}{V} \frac{d}{dt} I = -\frac{2D_L \Omega}{kT} \left(\frac{2\gamma_s A}{3V} - \bar{p} \right) \quad (16)$$

For a sphere the equivalent pressure is the same as the Laplace pressure $\bar{p} = -\gamma_s \kappa = 2\gamma_s A/3V$. In non-spherical particles it is $\bar{p} < 2\gamma_s A/3V$; then, Eq. (16) reduces the second moment of inertia.

2.2. Surface diffusion

The morphology of a particle evolves by surface diffusion. The surface motion can occur by atoms moving along the surface. The diffusive flux j_s is proportional to the gradient of the curvature:

$$j_s = -\frac{\gamma_s \delta D_s}{kT} \frac{1}{\Omega} \nabla_s \mu = \frac{\gamma_s \delta D_s}{kT} \nabla_s \kappa \quad (17)$$

where ∇_s denotes the surface gradient and δD_s is the surface diffusion coefficient multiplied by the surface thickness. The normal velocity v_n is the rate of accumulation of matter, which is the negative of the surface divergence of the flux by multiplying by Ω:

$$\Omega \nabla_s \cdot j_s = -v_n \quad (18)$$

Then

$$v_n = -\frac{\gamma_s \Omega \delta D_s}{kT} \nabla_s^2 \kappa \quad (19)$$

where ∇_s^2 denotes the surface Laplacian (also called the Laplace–Beltrami operator). This equation was originally proposed by Mullins [32], and termed the motion by the negative of the surface Laplacian of the mean curvature [33].

From the relation

$$\nabla \cdot (x_i x_j \boldsymbol{v}) = x_i x_j \frac{\partial v_k}{\partial x_k} + x_i v_j + v_i x_j \quad (20)$$

and the divergence theorem, we have

$$\frac{d}{dt} I_{ij} = \int_V (x_i v_j + v_i x_j) dV = \int_A x_i x_j v_n dA \quad (21)$$

Here we assume mass conservation inside the particle:

$$\partial v_k / \partial x_k = 0 \quad (22)$$

By substituting Eq. (19) into Eq. (21), and using a version of Green's theorem, we get

$$\int_A x_i x_j \nabla_s^2 \kappa dA = \int_A \kappa \nabla_s^2 (x_i x_j) dA \quad (23)$$

Here we use the formula $\nabla_s^2 (x_i x_j) = x_i \nabla_s^2 x_j + 2\nabla_s x_i \cdot \nabla_s x_j + x_j \nabla_s^2 x_i$, and the relation $\nabla_s x_i \cdot \nabla_s x_j = \delta_{ij} - n_i n_j$.

The curvature times the unit normal is related to the position by the surface Laplacian $\kappa n_i = \nabla_s^2 x_i$. We have the tensor virial equation for surface diffusion:

$$\frac{1}{V} \frac{d}{dt} I_{ij} = -\frac{\delta D_s \Omega}{kT} \Phi_{ij} \quad (24)$$

The driving force Φ_{ij} is

$$\Phi_{ij} = \frac{\gamma_s}{V} \int_A \left(x_i \kappa^2 n_j + x_j \kappa^2 n_i + 2\kappa(\delta_{ij} - n_i n_j) \right) dA \quad (25)$$

This tensor has the physical dimensions of force per unit volume. We shall call Φ_{ij} the surface force density.

The isotropic component is

$$\frac{1}{V} \frac{d}{dt} I = -\frac{\delta D_s \Omega}{kT} \frac{\gamma_s}{V} \left[\frac{2}{3} \int_A x_i \kappa^2 n_i dA + \frac{4}{3} \bar{\kappa} A \right] \quad (26)$$

The average curvature $\bar{\kappa}$ is given by

$$\bar{\kappa} = \frac{1}{A} \int_A \kappa dA \quad (27)$$

where A is the total surface area.

The rate of change of the surface area is [33,34]

$$\frac{dA}{dt} = -\frac{\gamma_s \Omega \delta D_s}{kT} \int_A |\nabla_s \kappa|^2 dS \quad (28)$$

This shows that surface motion reduces the total surface area.

3. Numerical simulation results

3.1. Surface Evolver program

The evolution of particle shape by surface diffusion was studied by using Brakke's Surface Evolver program [26]. The surface is represented as a set of triangular finite elements, or facets. Each facet consists of three edges and three vertices. The surface has energies proportional to its area. For the simulation of surface diffusion, the Surface Evolver program calculates the velocity of a vertex as the Laplacian of the mean curvature of the surface, Eq. (19), using the built-in Evolver method "Laplacian_mean_curvature". The mean curvature $\kappa/2$ at each vertex is calculated as a scalar. Then finite differences are used to calculate the Laplacian of the mean curvature. The actual motion is found by multiplying the velocity by a scale

factor. The physical interpretation of the scale factor is the time step. Modeling the dynamics of the evolution requires using a fixed time step. The sintering of two spheres by surface diffusion has been simulated accurately by utilizing the Surface Evolver program previously [14].

3.2. Spheroidization of a single particle

As a simple example, we consider the shape relaxation of an isolated ellipsoidal particle by surface diffusion. We restrict to axisymmetric ellipsoids (spheroids, either oblate $c/a < 1$ or prolate $c/a > 1$) which have semi-axes $a = b$, c as shown in Fig. 1. The volume of the spheroid is $V_0 = 4\pi a^2 c/$

3. The radius and the area of the equivalent sphere are $r_0 = (a^2 c)^{\frac{1}{3}}$ and $A_0 = 4\pi r_0^2$, respectively. The moment of inertia tensor of a spheroid is given by $I_{11} = I_{22} = V_0 a^2/5$, $I_{33} = V_0 c^2/5$, and plotted as a function of axial ratio c/a in Fig. 1. The second moment of inertia I is a minimum at $c/a = 1$. The deviatoric component $I_{33} - I_{11}$ increases with increasing magnitude of the anisotropy $c/a - 1$.

While the analytical expression of the surface energy tensor for ellipsoids has been given by Rosenkilde [35], it can be evaluated numerically by Surface Evolver. The surface energy tensor per volume $2S_{ij}/V_0$ is plotted in Fig. 2. The hydrostatic component is $2S_{ii}/3V_0 = 2\gamma_s A/3V_0$. Its
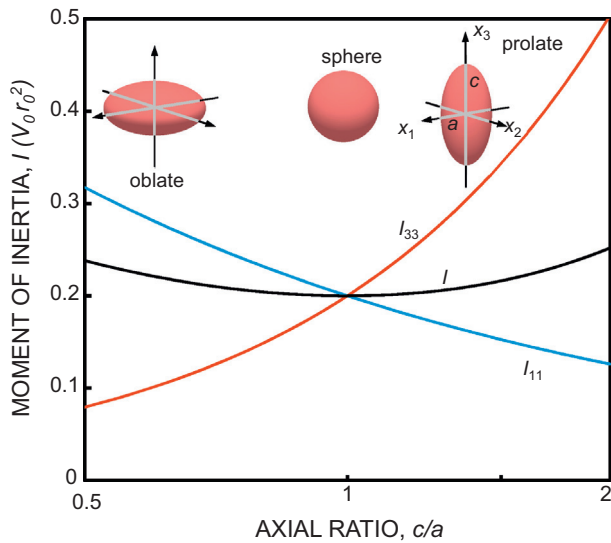

Fig. 1. Moment of inertia tensor of an axisymmetric ellipsoid (spheroid) as a function of the axial ratio (c/a). The isotropic and deviatoric components show the compactness and the anisotropy of the particle, respectively.

Fig. 3. Surface force density (Eq. (25)) of spheroid as a function of the axial ratio (c/a). It is the driving force of the moment of inertia tensor (Eq. (24)) in the microstructural evolution by surface diffusion.
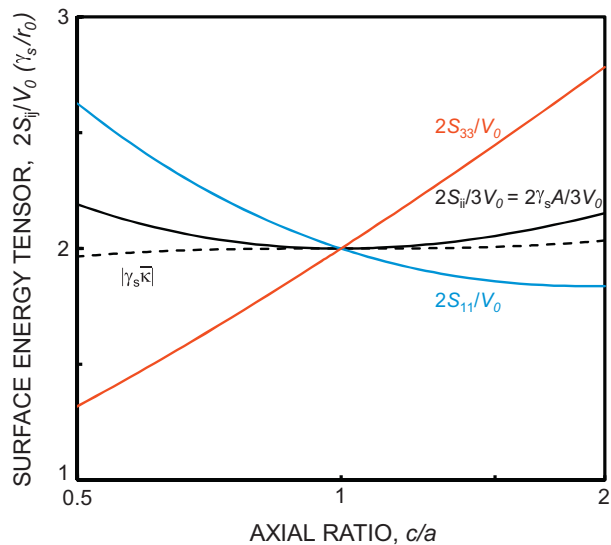

Fig. 2. Surface energy tensor of a spheroid as a function of the axial ratio (c/a). It is the driving force of the moment of inertia tensor in the microstructural evolution by bulk diffusion (Eq. (13)). The broken line shows the stress related to the average of curvature.
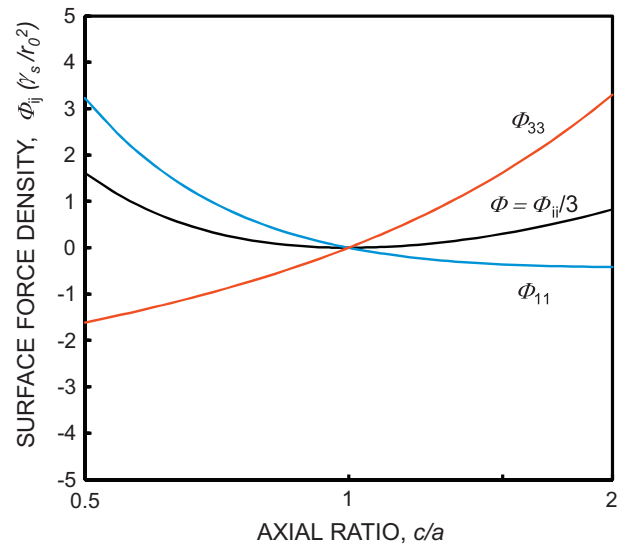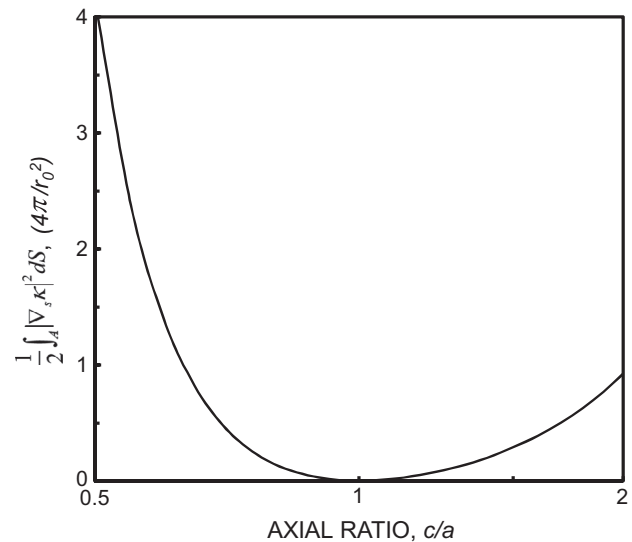

Fig. 4. Integral of the square of the gradient of the curvature, which is the driving force for the reduction of surface area by surface diffusion (Eq. (28)).

minimum is at $c/a = 1$, because a sphere has the minimum area under the constraint of fixed volume. The average surface stress $|\gamma_s\bar{\kappa}|$ defined by the average of surface curvature is also plotted in Fig. 2. They coincide with the Laplace pressure at equilibrium, i.e. a sphere. In non-equilibrium shapes, $2\gamma_sA/3V_0$ is always higher than $|\gamma_s\bar{\kappa}|$.

The surface force density Φ_{ij} is calculated numerically, and plotted in Fig. 3. Φ_{ij} acts so as to make an anisotropic particle more isotropic and more compact. The Surface Evolver program calculates the integral of the square of the gradient of the mean curvature, which is proportional to the rate of decrease in total area (Eq. (28)). It is plotted in Fig. 4. The integral becomes zero when the surface reaches the equilibrium state that has a constant mean curvature.

An oblate spheroid (initial axial ratio $c/a = 0.5$) evolves to be a sphere in equilibrium. The diagonal components of the moment of inertia tensor are plotted as a function of the dimensionless time:

$$t^* = \frac{\gamma_s\Omega\delta D_s}{kTr^4}t \tag{29}$$

in Fig. 5a. All diagonal components become $I_{eq} = 0.2V_0r_0^2$ in equilibrium. Fig. 5b shows the relation between the rate of change of the second moment of inertia and its driving force Φ_{ij} in the Surface Evolver simulation. The result proves that the tensor virial equation, Eq. (24), holds true in the simulation.
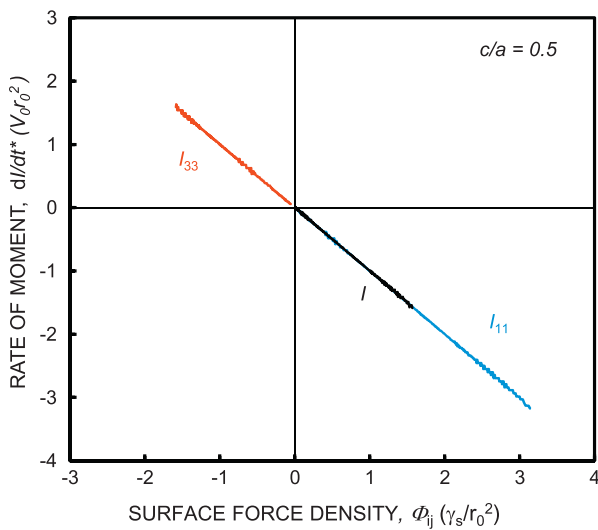
Fig. 6a shows that all components of the surface energy tensor become the same $2S_{eq}/V_0 = 2\gamma_s/r_0$ at the equilib-
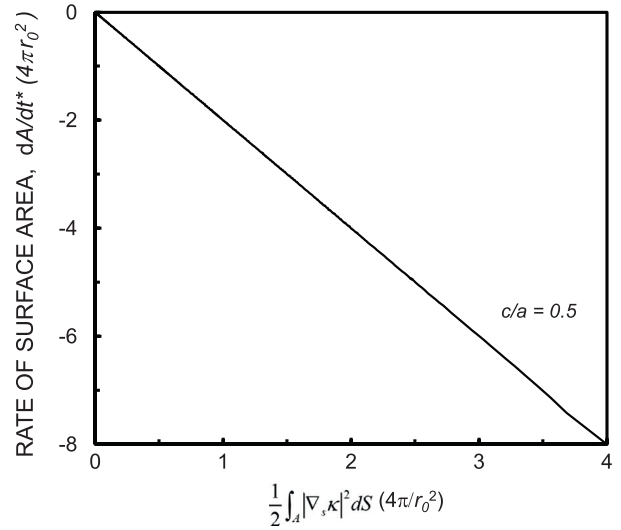

(a)
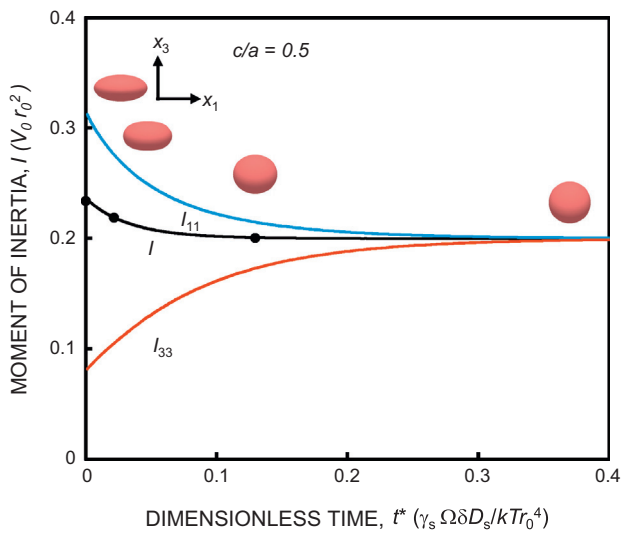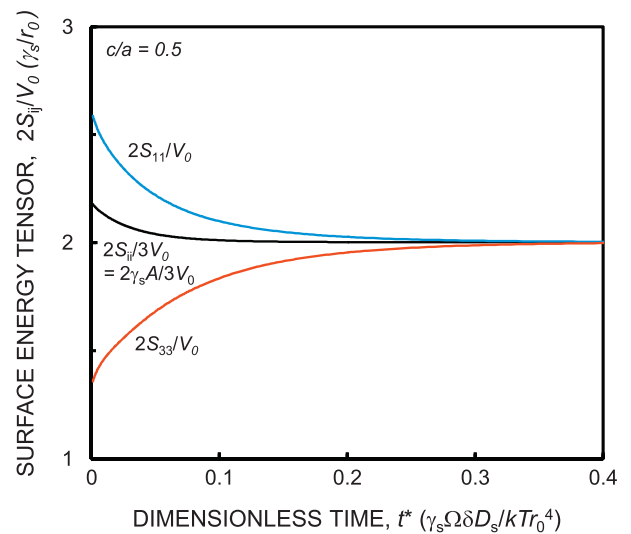
(b)

Fig. 5. Moment of inertia tensor during the spheroidization of an oblate spheroid (initial axis ratio $c/a = 0.5$) by surface diffusion. (a) Relaxation curve, (b) relation between the rate of moment of inertia and the surface force density.
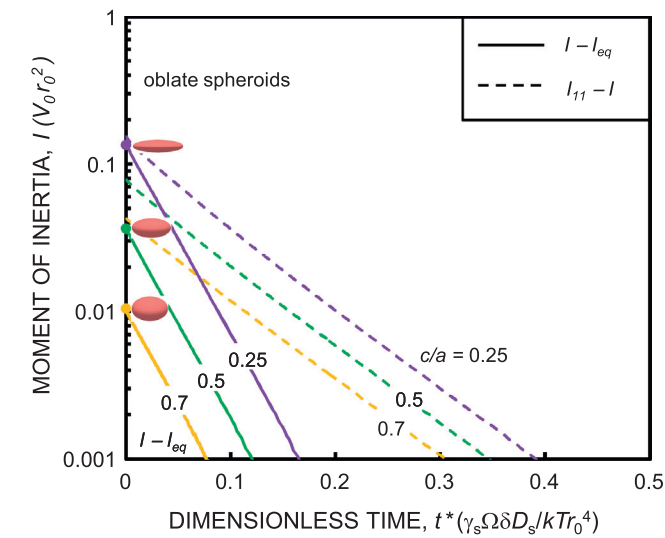

(a)

(b)

Fig. 6. Surface energy tensor during the spheroidization of an oblate spheroid (initial axis ratio $c/a = 0.5$) by surface diffusion. (a) Relaxation curve, (b) relation between the surface area and the integral of the square of the gradient of the curvature.

rium. The isotropic component decreases with time, indicating that the surface area is minimized in the simulation. The rate of area reduction is linearly proportional to the integral of the square of the gradient of the curvature, as shown in Fig. 6b. This is a proof that the Surface Evolver program simulates the morphological evolution by surface diffusion (Eq. (28)) correctly.
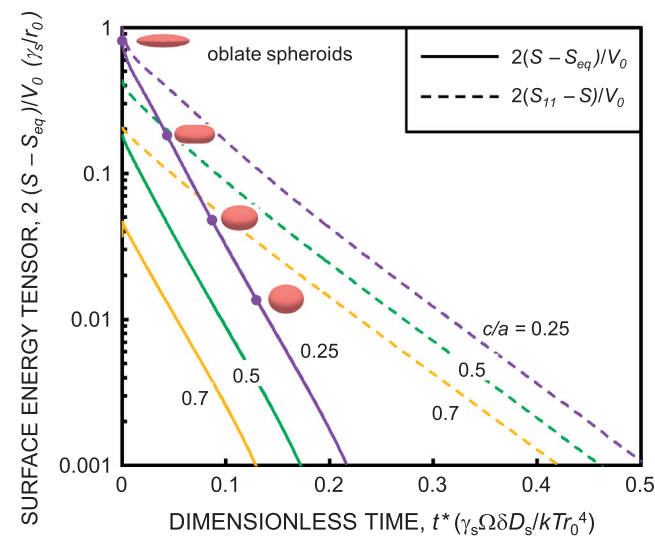
The isotropic and deviatoric components of the moment of inertia tensor are plotted in Fig. 7a with a logarithmic vertical axis. For oblate spheroids the kinetics follow the exponential decay law:

$$I - I_{eq} = (I_0 - I_{eq}) \exp\left(-\frac{t^*}{\tau^*}\right) \quad (30)$$

where I_0 is the initial value and τ^* is the dimensionless relaxation time. The relaxation time scales as $\tau = \tau^* kTr_0^4/\gamma_s \Omega \delta D_s$.

The dimensionless relaxation time of the isotropic component $\tau^* = 0.032$ was almost independent of the initial c/a in the range $0.5 \leqslant c/a < 1$. The relaxation time of the deviatoric component $I_{11} - I$ was $\tau^* = 0.081$, which was 2.5 times longer than that of the isotropic component. The components of the surface energy tensor are shown in Fig. 7b. The relaxation times of the surface energy tensor were almost the same as those of the moment of inertia tensor. The isotropic component decays much faster than the anisotropic components for both the surface energy tensor and the moment of inertia tensor.

For prolate spheroids the moment of inertia and the surface energy tensor do not follow the exponential decay law, as shown in Fig. 8. The shape profiles of Fig. 8b depict the process of blunting the elongated spheroid with the initial $c/a = 8$. The tips of the particle blunt and form bulbs on
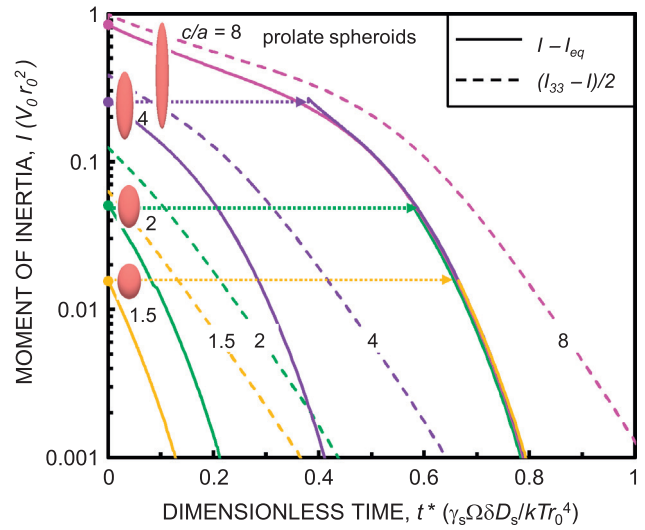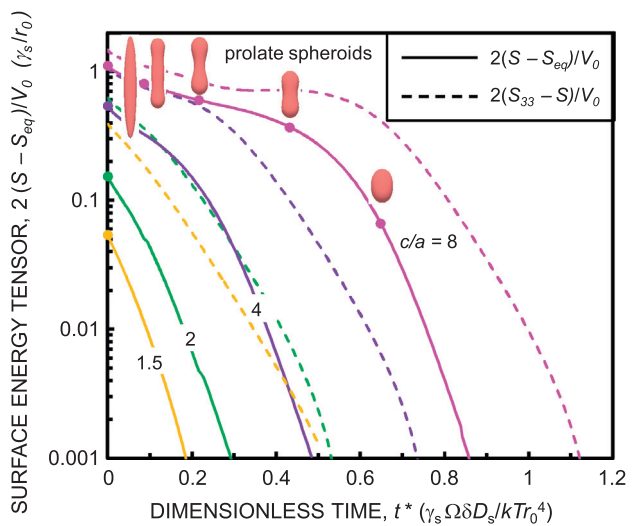

Fig. 7. Relaxation of oblate spheroids by surface diffusion: (a) moment of inertia tensor, (b) surface energy tensor. The kinetics follow an exponential decay law.

Fig. 8. Relaxation of prolate spheroids by surface diffusion: (a) moment of inertia tensor, (b) surface energy tensor. The relaxation curve at an initial axial ratio can be shifted to overlap with other curves in the later stage of sintering.

both ends. A neck is transiently formed between them, and then the ellipsoidal shape is recovered to evolve toward a sphere. In the region of ellipsoidal evolution, the curves for different initial axis ratio $1 \leqslant c/a < 4$ can be superposed by the horizontal shift, as shown in Fig. 8a.

3.3. Sintering of multi-particle aggregates

3.3.1. Particle pair

The fundamental process in sintering is studied by using Frenkel's model [36], the sintering of two identical spheres of radius r_0. We consider the coalescence of two particles by surface diffusion under the assumption of zero grain boundary energy. The evolution of the surface energy tensor and the moment of inertia tensor is shown in Fig. 9. The surface area reduces rapidly by neck growth in the initial stage of sintering, as shown in Fig. 9a. This stage ends at around $t^* = 0.1$, and spheroidization follows in the later stage. The surface energy tensor of two separated particles is isotropic. After a neck is formed, the deviatoric component increases in the initial stage, and decreases during the spheroidization period. The moment of inertia decreases with time in Fig. 9b, that is, the particle pair shrinks as it coalesces to be a sphere. Fig. 9c shows that the deviatoric component of the surface force density emerges after the neck is formed. The deviatoric component, which develops in the initial stage, becomes the driving force to make the particle pair more isotropic in the later stage.
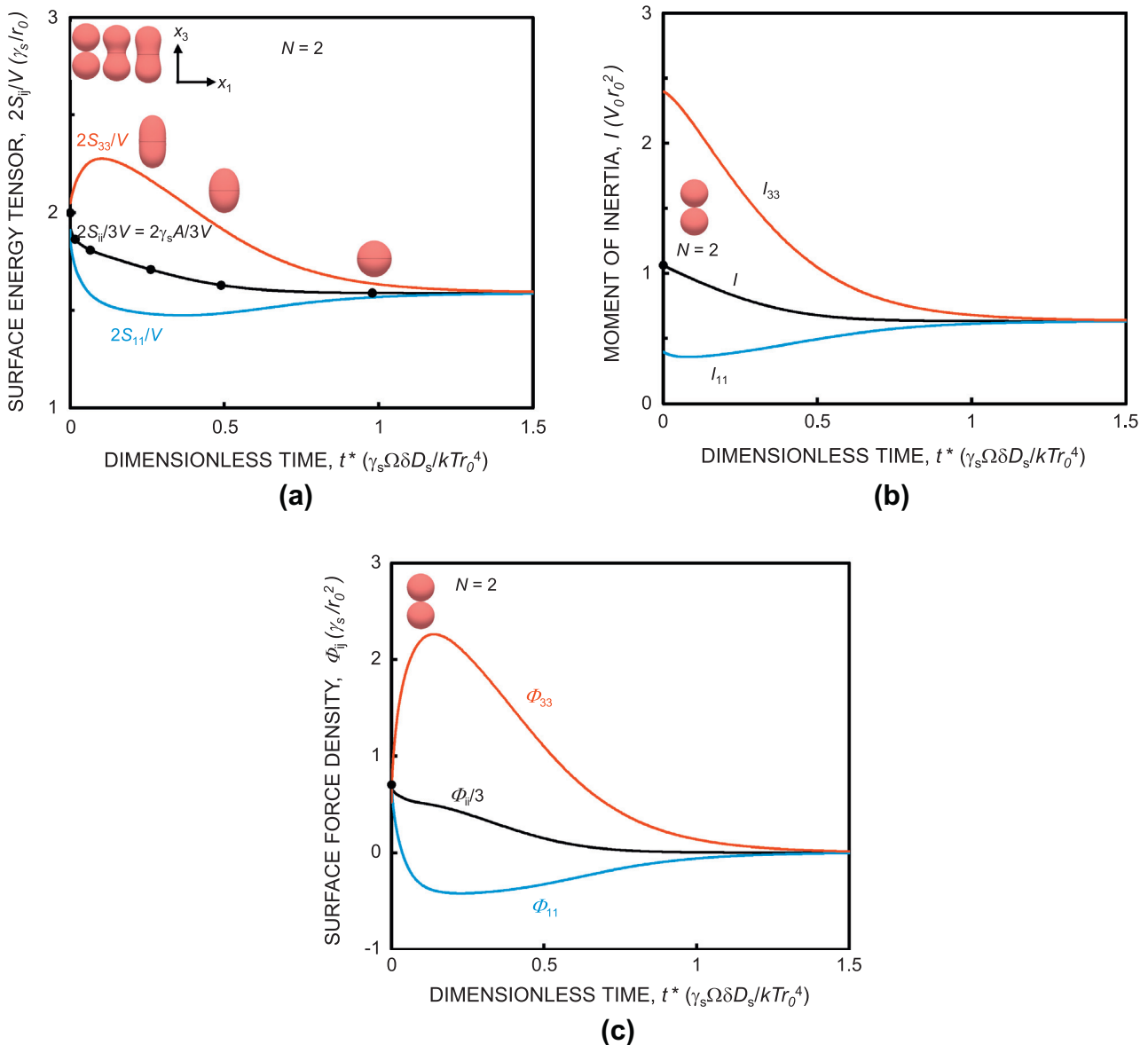

Fig. 9. Sintering of two identical spheres by surface diffusion: (a) surface energy tensor, (b) moment of inertia tensor, (c) surface force density. The deviatoric components increase with the neck growth in the initial stage of sintering.
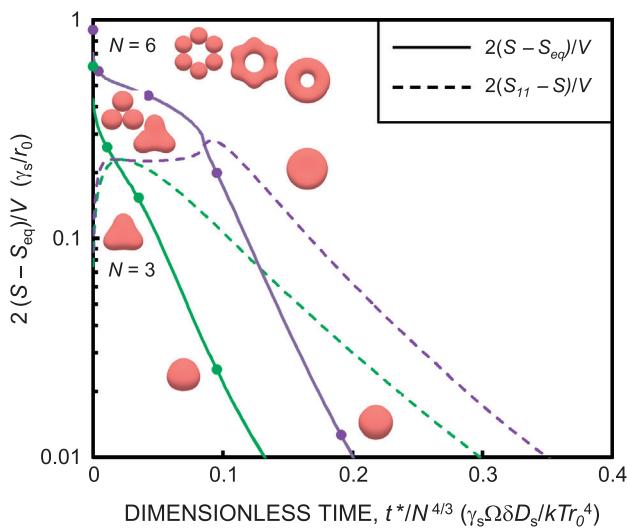
3.3.2. Ring of particles

An aggregate of N primary particles coalesces to be a sphere of radius $r = N^{1/3}r_0$ with volume $V = NV_0$ ultimately. The moment of inertia of the aggregate scales as $N^{5/3}$. We use the normalized moment of inertia $I/N^{5/3}$ and the normalized dimensionless time $t^* N^{4/3}$ in describing the sintering of multi-particle aggregates.

The elementary process of pore channel closure can be analyzed by using a ring of spheres, as shown in Fig. 10a. For a ring of six spheres, the sintering process is divided into three stages: the initial stage where necks grow until the ring becomes a torus (or doughnut shape), the intermediate stage where the hole shrinks and the final stage where the formed disk evolves to be a sphere in a way similar to the oblate spheroid. These three stages are distinguished by the slope of the surface energy tensor curve that

is related to the relaxation time. The slope is steep in the initial stage, gentle in the intermediate stage and moderately steep in the final stage. In the moment of inertia curves in Fig. 10b, only the intermediate stage and the final stage are distinguished, because the neck growth in the initial stage does not affect the moment of inertia significantly. The relaxation time in the final stage scaled by the number of spheres in the ring is $\tau^* = 0.032N^{4/3}$ for the isotropic component and $\tau^* = 0.081N^{4/3}$ for the deviatoric component.
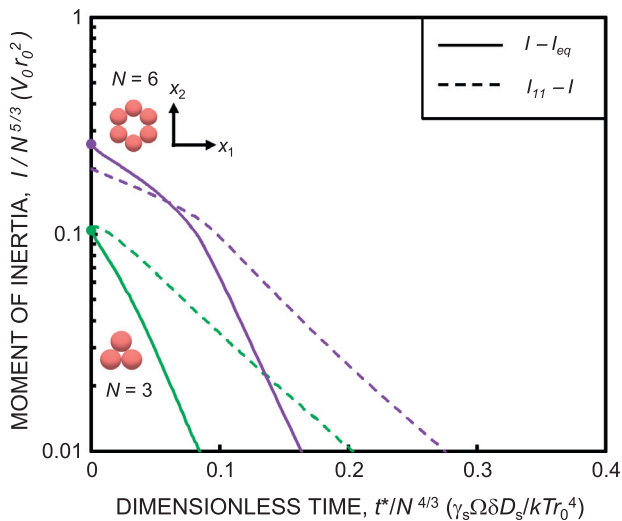
3.3.3. Chain of particles

The three stages are also observed in the sintering of a linear chain of particles ($N = 3$) in Fig. 11a: the initial stage where the necks between particles grow until the chain becomes a rod, the intermediate stage where a neck is
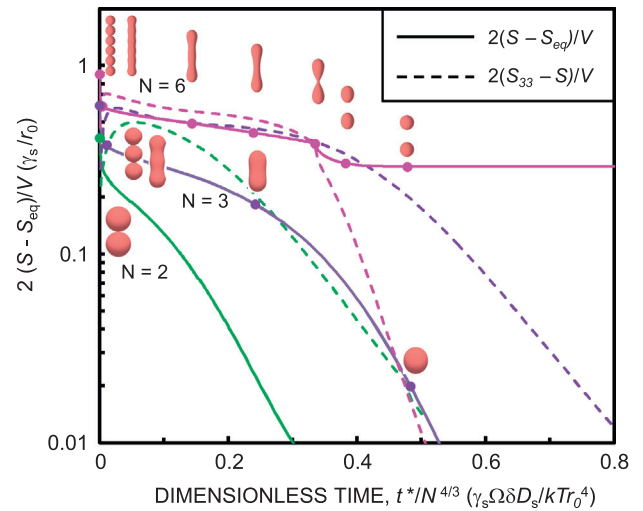
Fig. 10. Sintering of rings of particles by surface diffusion: (a) surface energy tensor, (b) moment of inertia tensor. The coalesced particle evolves in a way similar to oblate spheroids in the final stage.
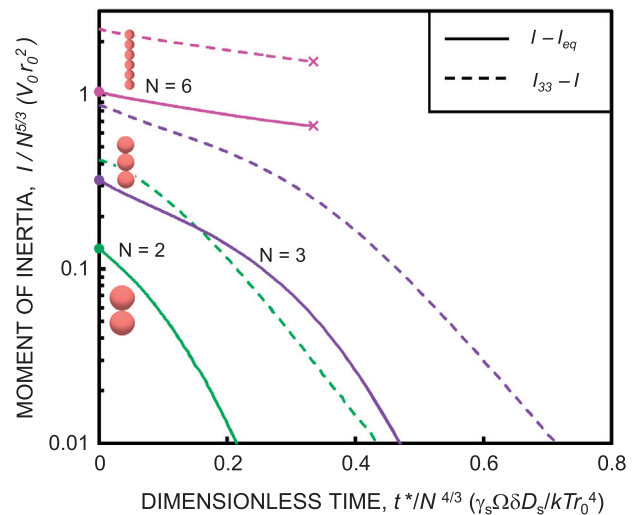

Fig. 11. Sintering of chains of particles by surface diffusion: (a) surface energy tensor, (b) moment of inertia tensor. The coalesced particle evolves in a way similar to prolate spheroids in the final stage. The chain with $N = 6$ breaks up to form two spheres.
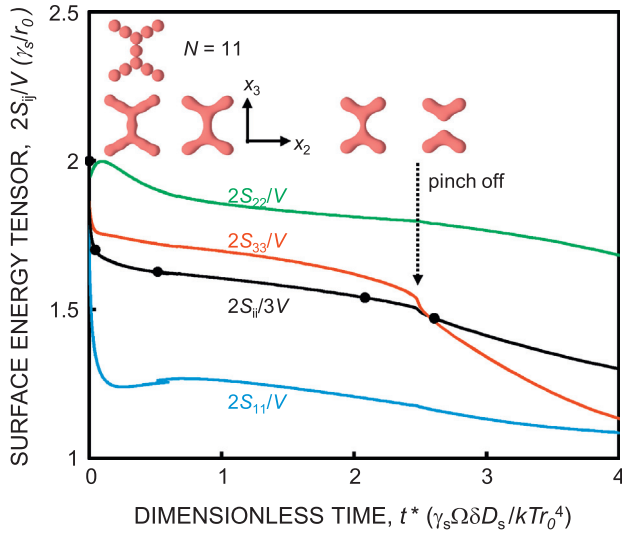
Fig. 12. Sintering of a branched chain of particles. The symmetry of the aggregate changes from orthorhombic to tetragonal, and finally isotropic structure.

formed transiently between bulbs on both ends and the final stage where the prolate spheroid evolves to be a sphere. In the intermediate sintering of the chain of six spheres, the rod is unstable so that it breaks up to form two spheres. This pinch-off is analogous to Rayleigh instability of a cylinder of fluid under capillary force, as has been analyzed by Nichols and Mullins [20], Nichols [37] and Bernoff [34]. The two separated spheres are metastable, and the sum of their surface energy is higher than the single coalesced sphere.

The relaxation times in the intermediate stage are calculated from the slopes of the moment of inertia curves in Fig. 11b. They are $\tau^* = 1.0$ and $\tau^* = 7.5$ for $N = 3$ and $N = 6$, respectively. The relaxation time in the intermediate stage was much longer than that in the final stage.

3.3.4. Branched chain of particles

Agglomerates made by diffusion-limited aggregation have branched-chain structures [38]. The shape evolution of a branched chain of particles ($N = 11$) is shown in Fig. 12. Each branch has a finger-like shape in the intermediate stage, and the central neck pinches off later. The fragments become prolate spheroids, and two spheres are formed ultimately. The three different components of surface energy tensor show the transition in symmetry of the structure: from orthorhombic ($S_{11} \neq S_{22} \neq S_{33}$) to tetragonal ($S_{11} = S_{33} \neq S_{22}$) and finally to isotropic ($S_{11} = S_{33} = S_{22}$) structures.

4. Discussion

4.1. Coupling between the moment of inertia and the surface energy tensor

In sintering by surface diffusion, the moment of inertia tensor and the surface energy tensor are treated separately.

The rate of change of the moment of inertia is proportional to the isotropic component of force density tensor Φ. The comparison between Figs. 2 and 3 shows that Φ is approximately proportional to $2S_{ii}/3V - 2$ only for oblate spheroids ($0.25 \leqslant c/a \leqslant 1$).

On the other hand, in sintering by bulk diffusion, the moment of inertia tensor is directly coupled with the surface energy tensor in Eq. (13). In viscous sintering, the deformation of an ellipsoidal particle is driven by the surface energy tensor [5]

$$2\mu\dot{e}_{ij} = \frac{2\gamma_s A}{3V}\delta_{ij} - \frac{2S_{ij}}{V} \tag{31}$$

where $\dot{e}_{ij}$ is the strain rate and μ is the viscosity. The rate of change of the moment of inertia tensor of a spheroid is directly related to the surface energy tensor, because

$$\frac{dI_{11}}{dt} = -\frac{2Va^2}{5}\dot{e}_{11}, \quad \frac{dI_{33}}{dt} = -\frac{2Vc^2}{5}\dot{e}_{33} \tag{32}$$

4.2. Relaxation time for the exponential decay

Nichols and Mullins [20] gave solutions for the relaxation of bodies slightly perturbed from spherical geometries. They considered a small perturbation in the radius of a sphere:

$$r = r_0 + q_l Y_{lm}(\theta, \phi) \tag{33}$$

where Y_{lm} are spherical harmonics and $q_l \ll r_0 =$ unperturbed radius of sphere. For surface diffusion, the relaxation time for the exponential decay of the perturbation q_l is given as

$$\tau^* = 1/l(l+1)(l-1)(l+2) \tag{34}$$

The relaxation time will be $\tau^* = 0.042$ for $l = 2$. This is just half of the relaxation time for deviatoric components of the surface energy tensor and the moment of inertia tensor for oblate spheroids.

The shape of a particle can be described by the expansion coefficients q_l in terms of spherical harmonic functions. Frenkel [36] showed that the surface area is given by the expansion coefficients

$$A - A_0 = \sum_l (l-1)(l+2)q_l^2 \tag{35}$$

The relaxation time of the surface area will be half of that of q_l. This is the reason why the relaxation time of the isotropic component of surface energy tensor is shorter than that of the deviatoric components. The exponential decay of small perturbation has been analyzed also for bulk diffusion [20] and viscous flow [36,39].

Koch and Friedlander [40] proposed the exponential decay law of surface area for aggregates in viscous sintering. Their model agrees well with simulation results on sintering of two identical spheres by viscous flow [7,10]. However, in the sintering of aggregates by surface diffusion, the surface area does not follow simple exponential decay law, as shown in Figs. 10a and 11a.

Finally it should be mentioned that the morphological evolution of a spheroidal particle is also characterized by its axial ratio. Tanaka [41] proposed a rate equation for the axial ratio in spheroidization by diffusion. The axial ratio is expressed as a function of I_{33}/I_{11}, and vice versa.

5. Summary

Sintering and coalescence make the aggregates of primary particles become more compact and more isotropic structures. The morphology of an aggregate was characterized by the moment of inertia tensor: the isotropic component showed the compactness, and the deviatoric component showed the anisotropy. We proposed the tensor virial equation for evolving particles by diffusion. In microstructural evolution by bulk diffusion, the moment of inertia tensor was driven by the surface energy tensor. The surface force density was identified as the driving force of the moment of inertia tensor for the case of surface diffusion. The evolution of aggregates by surface diffusion was simulated by the Surface Evolver program. For an isolated single oblate spheroidal particle, both the moment of inertia tensor and the surface energy tensor followed the exponential decay law. In the sintering of two identical spheres, the deviatoric components of the surface force density developed in the initial stage where the neck grew rapidly. The generated deviatoric component became the driving force of spheroidization in the later stage. The simulation of aggregates or particles (ring, linear chain and branched chain) showed that various topological transformations could be described by using the moment of inertia tensor and the surface energy tensor.

References

[1] Parker EN. Phys Rev 1954;96:1686.
[2] Marc G, McMillan WG. Adv Chem Phys 1985;58:209.
[3] Chandrasekhar S. Proc R Soc Lond A 1965;286:1.
[4] Rosenkilde CE. J Math Phys 1967;8:84.
[5] Wakai F, Shinoda Y, Akatsu T. J Am Ceram Soc 2012;95:2785.
[6] Schmid HJ, Tejwani S, Artelt C, Peukert W. J Nanoparticle Res 2004;6:613.
[7] Kirchhof MJ, Schmid HJ, Peukert W. Phys Rev E 2009;80:026319.
[8] Hawa T, Zachariah MR. Phys Rev B 2007;76:054109.
[9] Fry D, Mohammad A, Chakrabarti A, Sorensen CM. Langmuir 2004;20:7871.
[10] Eggersdorfer ML, Kadau D, Herrmann HJ, Pratsinis SE. Langmuir 2011;27:6358.
[11] Coble RL. J Am Ceram Soc 1958;41:55.
[12] Johnson DL. J Appl Phys 1969;40:192.
[13] Beere W. Acta Metall 1975;23:139.
[14] Wakai F, Brakke KA. Acta Mater 2011;59:5379.
[15] Svoboda J, Riedel H, Zipse H. Acta Metall Mater 1994;42:435.
[16] Wakai F, Shinoda Y. Acta Mater 2009;57:3955.
[17] Herring C. In: The Physics of Powder Metallurgy. New York: McGraw-Hill; 1951. p. 143.
[18] Ross JW, Weatherly GC. Z Metallkde 1982;73:391.
[19] Nichols FA, Mullins WW. J Appl Phys 1965;36:1826.
[20] Nichols FA, Mullins WW. Trans Metall Soc AIME 1965;233:1840.
[21] Bruchon J, Drapier S, Valdivieso F. Int J Numer Meth Eng 2011;86:845.
[22] Kingery WD, Berg M. J Appl Phys 1955;26:1205.
[23] Wakai F, Aldinger F. Acta Mater 2003;51:4013.
[24] Manoharan VN, Elsesser MT, Pine DJ. Science 2003;301:483.
[25] Lauga E, Brenner MP. Phys Rev Lett 2004;93:238301.
[26] Brakke KA. Exp Math 1992;1:141.
[27] Karnesky RA, Sudbrack CK, Seidman DN. Scripta Mater 2007;57:353.
[28] Midgley PA, Weyland M. Ultramicroscopy 2003;96:413.
[29] Holzer L, Muench B, Wegmann M, Gasser P. J Am Ceram Soc 2006;89:2577.
[30] Ketcham RA. J Struct Geol 2005;27:1217.
[31] Herring C. J Appl Phys 1950;21:437.
[32] Mullins WW. J Appl Phys 1957;28:333.
[33] Cahn JW, Taylor JE. Acta Metall Mater 1994;42:1045.
[34] Bernoff AJ, Bertozzi AL, Witelski TP. J Stat Phys 1998;93:725.
[35] Rosenkilde CE. J Math Phys 1967;8:88.
[36] Frenkel J. J Phys USSR 1945;9:385.
[37] Nichols FA. J Mater Sci 1976;11:1077.
[38] Witten Jr TA, Sander LM. Phys Rev Lett 1981;47:1400.
[39] Hopper RW, Uhlmann DR. Mater Sci Eng 1974;15:137.
[40] Koch W, Friedlander SK. J Colloid Interface Sci 1990;140:419.
[41] Tanaka H. J Eur Ceram Soc 2004;24:2763.